



Research paper

Upgraded **GROWTH 3.0** software for structural gravity inversion and application to El Hierro (Canary Islands)

Antonio G. Camacho ^a, Juan F. Prieto ^b, Alfredo Aparicio ^{a,1}, Eumenio Ancochea ^c, José Fernández ^{a,*}

^a Instituto de Geociencias (CSIC, UCM), Calle del Doctor Severo Ochoa, nº 7. Edificio Entrepabellones 7 y 8, Ciudad Universitaria, 28040, Madrid, Spain

^b E.T.S. de Ingenieros en Topografía, Geodesia y Cartografía, Universidad Politécnica de Madrid, 28031, Madrid, Spain

^c Departamento de Mineralogía y Petrología, Fac. CC. Geológicas, Universidad Complutense de Madrid, 28040, Madrid, Spain

ARTICLE INFO

ABSTRACT

Keywords:

Gravity anomaly
Data inversion
Gravity inversion software
3D crustal models
El Hierro
Canary Islands

GROWTH 3.0 is a software package to determine the subsurface 3D density distribution that adjust discrete gravity anomaly values determined from gravity observations. The software uses very general assumptions and quite automatically determines the 3D density structures described by the aggregation of thousands of small rectangular prisms. A previous version of the software was published in 2011. However, methodological developments and computational technical evolution made it necessary to upgrade the software to include new advances and recent improvements in the inversion methodology (automatic determination of density contrasts, background medium with downward density increase, etc.), and a change in the computer operating system (from Windows XP, which was compatible with the 2011 version, to Windows 10 Pro for the current version). Here we describe the new upgraded version of the software package (which can be downloaded free), its use and application, using the study of El Hierro (Canary Islands) as a test case from which to obtain a 3D density model of its crustal structure. We also give a brief geological and volcanological interpretation.

1. Introduction

The determination of mass distribution in the subsoil from gravimetric anomaly values (gravity inversion) poses two basic problems: the inherent non-uniqueness of solution, and the fact that the data are inaccurate values obtained at a small number of non-uniformly distributed points. In addition, gravity data may be affected by regional components. Both basic problems can be solved by adding additional constraints in regard to: (1) on the model parameters (e.g., available information on the subsurface structure from petro-physical properties, structural orientations, geo-statistical information and mathematical hypothesis such as shape of a target); and (2) the data parameters (statistical properties of the inexact data, e.g., Gaussian distribution of errors). Mathematical constraints are usually exercised by minimizing a function involving the parameters of the assumed interpretation model (e.g., Farquharson et al., 2008; Lelievre and Oldenburg, 2009), including the volume of the causative body (e.g., Last and Kubik, 1983), minimum source moment of inertia (e.g., Guillen and

Menichetti, 1984), or minimum distance, flatness, smoothness and compactness (e.g., Barbosa and Silva, 1994; Boulanger and Chouteau, 2001; Ghalehnoee et al., 2017).

Another way of classifying gravity inversion methods is to consider the unknown type. Some studies consider density values as the unknown model parameters (e.g., Li and Oldenburg, 1998; Bertete-Aguirre et al., 2002; Ghalehnoee et al., 2017), in what is known as the linear approach. In other methods the parameters to be adjusted are geometric (non-linear approach), such as the depth of a discontinuity surface (e.g., Martins et al., 2011; Mojica and Bassrei, 2015; Santos et al., 2015), polyhedral structures (e.g., Wildman and Gazonas, 2009; Oliveira and Barbosa, 2013), or the aggregation of small cells (e.g., Krahnenbuhl and Li, 2006). Other interesting methodological approaches has also been developed, and include the stochastic approach (which combines several kinds of geophysical data) (e.g., Shamsipour et al., 2012), the spectral approach (e.g., Zadro and Braatenberg, 1997), fuzzy entropy (e.g., Liu and Jin, 2020), the use of the Particle Swarm Optimization algorithm (Pallero et al., 2021), graph theory (Vatankhah et al., 2019) or

* Corresponding author.

E-mail address: jft@mat.ucm.es (J. Fernández).

¹ Retired & now at Dpto. de Geología. Museo Nacional de Ciencias Naturales. CSIC. Calle de José Gutiérrez Abascal, 2, 28006-Madrid, Spain.

<https://doi.org/10.1016/j.cageo.2021.104720>

Received 27 March 2020; Received in revised form 27 January 2021; Accepted 12 February 2021

Available online 17 February 2021

0098-3004/© 2021 The Authors.

Published by Elsevier Ltd.

This is an open access article under the CC BY-NC-ND license

(<http://creativecommons.org/licenses/by-nc-nd/4.0/>).

GPU parallel computing (Chen et al., 2015).

Gravity inversion has been largely used for geophysical exploration in a number of environments, ranging from archaeology (e.g., Linford, 2006) to the study of the continental crust and plate tectonics (e.g., Molina-Garza and Utrruitia-Fucugauchi, 1993). More common applications include mineral exploration (e.g., Lelièvre et al., 2012), hydrocarbons (e.g., Jiang et al., 2020) and the detection of salt bodies (e.g., Silva Dias et al., 2011).

Another interesting field of application is the study of volcanic areas (Deplus et al., 1995; Kauahikaua et al., 2000; Fournier et al., 2004; Gudmundsson and Hognadottir, 2007; Linde et al., 2017), where many common volcanic structures have density anomalies. Volcanic activity is often manifested by a surface deformation and variations in gravity (Fernández et al., 2017), whose interpretation requires theoretical models and inversion techniques, as well as the most detailed possible information on the crustal structure (Chavez-García et al., 2007; Fernández et al., 2015, 2017). The reconstruction of the magmatic plumbing system (as shown by a 3D distribution of densities) can be used to assess the magma paths at an active volcano (Tibaldi, 2015; Magee et al., 2018). All these aspects highlight the importance of knowing the crustal structure in volcanic areas. Gravimetric methods are one kind of the used ones to obtain this important information.

This work presents an updated and improved version of the GROWTH software package. This computational tool for 3D inversion of gravity data, which was introduced and described in detail with applications in previous works (Camacho et al., 2000, 2002, 2007; Gottsmann et al., 2008; Camacho et al., 2011a,b, 2015, 2019), is a general methodology that defines the subsurface mass structure as an aggregation of small cells filled with anomalous densities. Certain regularization conditions regarding the model size are added to get a valuable solution. This non-linear approach is solved by an exploration process working under scale factor, and can be applied in different geological environments (beyond the volcanic example here considered). Our aim is to ensure applicability by including in the inversion approach concepts such as regional trend, general downward density increase and layered structures.

2. Basic principles of the growth gravity inversion

Below is a brief description of the methodology used by the software (see previous references for more details).

The inversion methodology creates a 3D subsurface model by aggregating m parallelepiped cells. They are filled, in a “growth” process, with prescribed positive and negative density contrasts. The design equation for relating observables, i.e. the gravity anomaly Δg_i at n observation points (with coordinates (x_i, y_i, z_i)), with modelling parameters and residuals v_i is:

$$\Delta g_i \sum_{j \in J^+} A_{ij} \Delta p_j^+ + \sum_{j \in J^-} A_{ij} \Delta p_j^- + d g_{reg} + v_i , \quad i = 1, \dots, n , \quad (1)$$

where A_{ij} is the vertical attraction for unit density of the j -th cell at the observation point i -th (e.g., Pick et al., 1973); Δp_j^- , Δp_j^+ are negative and positive density variations for the j -th cell; J^+ , J^- are sets of indexes corresponding to filled cells with positive or negative density variations; v_i are residual values and $d g_{reg}$ is a regional component composed of an offset regional value g_0 and a linear trend.

Sets J^+ and J^- are the main unknowns to be determined during the inversion process. They establish which cells are filled with prescribed positive or negative density variations, and therefore determine the geometry of the 3D density anomalies. The statement of the inverse problem in geometric unknowns with prescribed density values (e.g., Krahenbuhl and Li, 2006) is a non-linear problem, as opposed to approaches in unknown densities (e.g., Bertete-Aguirre et al., 2002) which would initially correspond to a linear problem. The regional (linear) trend $d g_{reg}$ is optimally determined simultaneously with the inverse

determination of the local anomalous structures (Camacho et al., 2000). This approach avoids the frequent distortions deriving from a prior external calculation of the regional trend.

To solve the problem of non-uniqueness, we adopt a mixed minimization condition based on model “fitness” (least square minimization of residuals) and model “smoothness” (l_2 -minimization of total anomalous mass),

$$v^T Q_D^{-1} v + \lambda f^2 m^T Q_M^{-1} m = \min . \quad (2)$$

where $m = (\Delta \rho_1, \dots, \Delta \rho_m)^T$ (T represents transposed matrix) includes the density contrast values considered for the different cells in the model; $v = (v_1, \dots, v_n)^T$, is the residual values vector, Q_D denotes the a priori covariance matrix for uncertainties of the gravity anomaly data (set as a diagonal matrix of estimated variances derived from the observation and reduction process); Q_M denotes the a priori covariance matrix for uncertainties of the parameters of the model; λ is a factor for the selected balance between the fitness and the smoothness of the model; $\Delta \rho_j$ are the anomalous density values $\Delta \rho_j^+$ and $\Delta \rho_j^-$ and $f \geq 1$ is an unknown scale factor for fitting the modelled anomalies Δg_i^C to the observed anomalies Δg . The non-linear problem defined by equations (1) and (2) is resolved by model exploration. We set a diagonal matrix Q_M with elements q_j ($j = 1 \dots m$) corresponding to i -th cells, centered in (X_j, Y_j, Z_j) and with volume V_j , as given by:

$$q_j = \frac{V_j}{n} \sum_{i=1}^n \frac{|z_i - Z_j|}{r_{ij}^3} \quad (3)$$

where r_{ij} is the distance between cell j -th and observation point i -th.

Parameter λ allows a suitable balance between data fitting and l_2 -smoothness of the adjusted model. Low λ values produce very small final residuals (even with partial fitting of the observational noise), although the resulting inverse model become excessively large and geometrically complex (even with speculative or fictitious details). Conversely, high λ values provide simple (small, rounded, and within a conservative range) models, but data fit may be poor. In previous papers we propose to get a suitable choice criterion by analysing the autocorrelation of residual values.

Parameter f is an internal tool for resolving the non-linear problem by exploring the model space (Tarantola, 1988). Inverse models are formed by several thousands of cells, so exploring all the possible combinations of cells would be an extremely large process. The key to the present inversion process consists in substituting the entire model exploration with a step-by-step exploration of the model growth. For each particular step k cells have been filled, and they fit the observed data (and the smoothing conditions) only by means of a scale factor f_k . Now the approach seeks to fill only a new cell (by simply exploring all candidate cells). This new cell is adjusted by minimizing the observing and smoothing conditions, with only a new scale value f_{k+1} . The growth process continues (with smaller f values) filling the cells with prescribed positive or negative density values until f is close to 1. The introduction of the unknown scale factor f is a key element of the process.

The following are the main characteristics of the latest version of the published methodology (Camacho et al., 2019):

- ✓ solution for 3D model space,
- ✓ acceptance of non-gridded non-planar low-precision data,
- ✓ computation can be started considering an empty body or an initial “seed” structure,
- ✓ automatic determination of the regional gravity trend as a linear function obtained from the data,
- ✓ inversion considering both positive and negative density changes simultaneously,
- ✓ inversion for irregularly-shaped 3D distributions with different single bodies,
- ✓ semi-automated data inversion routine,

- ✓ input of model parameters by means of an easy dialogue screen offering default values (Fig. 1).

Some recent improvements (Camacho et al., 2019), coupled with the obsolescence of the operating system (Windows XP), prompted us to devise a new upgraded version of the software package.

3. Novelties of the new version

The upgraded version of the software **GROWTH 3.0** has been developed based on the earlier published versions (Camacho et al., 2000; 2011a, b; 2015) and incorporates the following new features:

- (a) it is adapted to run in the framework of the new Microsoft operating system (Windows 10 Pro),
- (b) a more compact package with only two codes,
- (c) optional automatic determination of the prescribed values for the density contrast,
- (d) optional inversion accounting for sub-horizontal layered structures,
- (e) optional inversion considering an increase in density with depth in the background medium,
- (f) new graphical presentation throughout the inversion process (Fig. 2),
- (g) simpler structure of the file with the resulting 3D model.

From a methodological point of view, the previously published software determined the 3D geometry of the distribution of density anomalies with respect to a homogeneous background medium. However, it does not provide a realistic representation, as the adjusted 3D structures may appear isolated and, in a shallow position, without a deep root. Alternatively, we could consider these anomalous 3D bodies as being included in a background medium with a general increase in density with depth. Expressed colloquially, this produces anomalous bodies with a bell shape rather than a hanging globe shape.

We have developed two alternative approaches, considering: (i) an initial background medium described by a discrete number of sub-horizontal layers (Camacho et al., 2011b) (improvement d), and (ii) an initial background medium with continuous downward density increase (Camacho et al., 2019) (improvement e). These two options can be summarized as follows:

(i) In this approach, the initial background model is described by

several sub-horizontal discontinuity interfaces, S_1, S_2, \dots , limiting (homogeneous) density layers. Initially, the interfaces are horizontal, at depths Z_1, Z_2, \dots . The idea is to determine an optimal topography of these interfaces (able to fit the data and the smoothing conditions) from the cells contiguous to the limiting surfaces for each growth step, and fill them with the density contrast between the upper and lower layers. In this mode the topographic details of the discontinuity surfaces grow from the initially flat discontinuity surfaces [see Camacho et al. (2011b) for a more detailed explanation and an illustrative figure]. This is done (Camacho et al., 2011b) by substituting the previously equation (2) by:

$$\mathbf{v}^T \mathbf{Q}_D^{-1} \mathbf{v} + \lambda f^2 \mathbf{m}^T \mathbf{P} \mathbf{Q}_M^{-1} \mathbf{m} = \min. \quad (4)$$

The diagonal weighting matrix \mathbf{P} has no null elements, P_{jj} , (with values P_{jj}^+, P_{jj}^- for negative and positive contrast) linearly depends on the vertical distance $z_j - Z_k$ from the cell k -th to the interface:

$$\begin{pmatrix} P_{jj}^+ \\ P_{jj}^- \end{pmatrix} = \begin{pmatrix} a_k^+ \\ a_k^- \end{pmatrix} (z_j - Z_k) + \begin{pmatrix} b_k^+ \\ b_k^- \end{pmatrix} \quad (5)$$

$a_k^-, a_k^+, b_k^-, b_k^+$ are coefficients for linearity.

This additional weighting matrix \mathbf{P} causes the cells adjacent to the discontinuity surfaces to be prioritised for filling. The main (but not the sole) activity of the growth process is therefore to build the discontinuity surface relief.

Here, j cell (with depth z_j) is located (above or below) close to k interface (with depth Z_k). Sign + or - indicates whether positive or negative density contrast values are being considered. Negative values below the interface serve to deepen it, and positive values above the interface serve for raise it. The coefficients $a_k^+ > 0$ and $a_k^- < 0$ control the resulting displacement (upward and downward respectively) of the interface and determine its flatness. See Camacho et al. (2011b) for more details.

(ii) This second approach considers that density contrast values do not remain fixed everywhere, but vary with depth (positive values increase downwards and negative values decrease downward, around the middle depths of the sensitive zone). This downward increase/decrease can be assumed to be linear or, at best, exponential. This is formulated by writing the variable positive or negative density increment values $\Delta\rho_j^+$ and $\Delta\rho_j^-$ as given, for the j -th cell at the k -th step, by (Camacho et al., 2019):

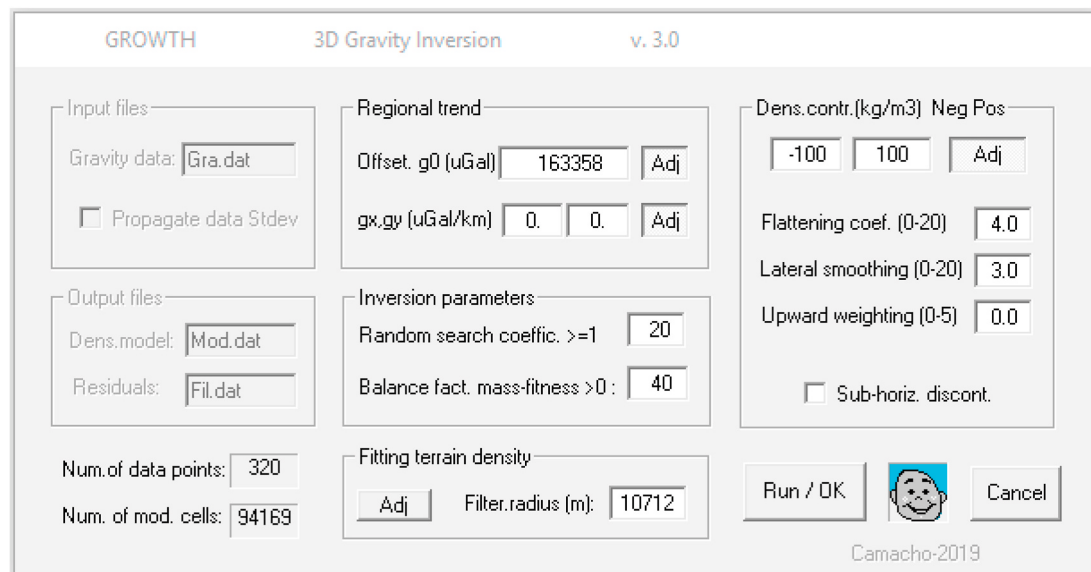


Fig. 1. Example of dialogue screen for users to input the inversion parameters, including suggestions of default parameters values.

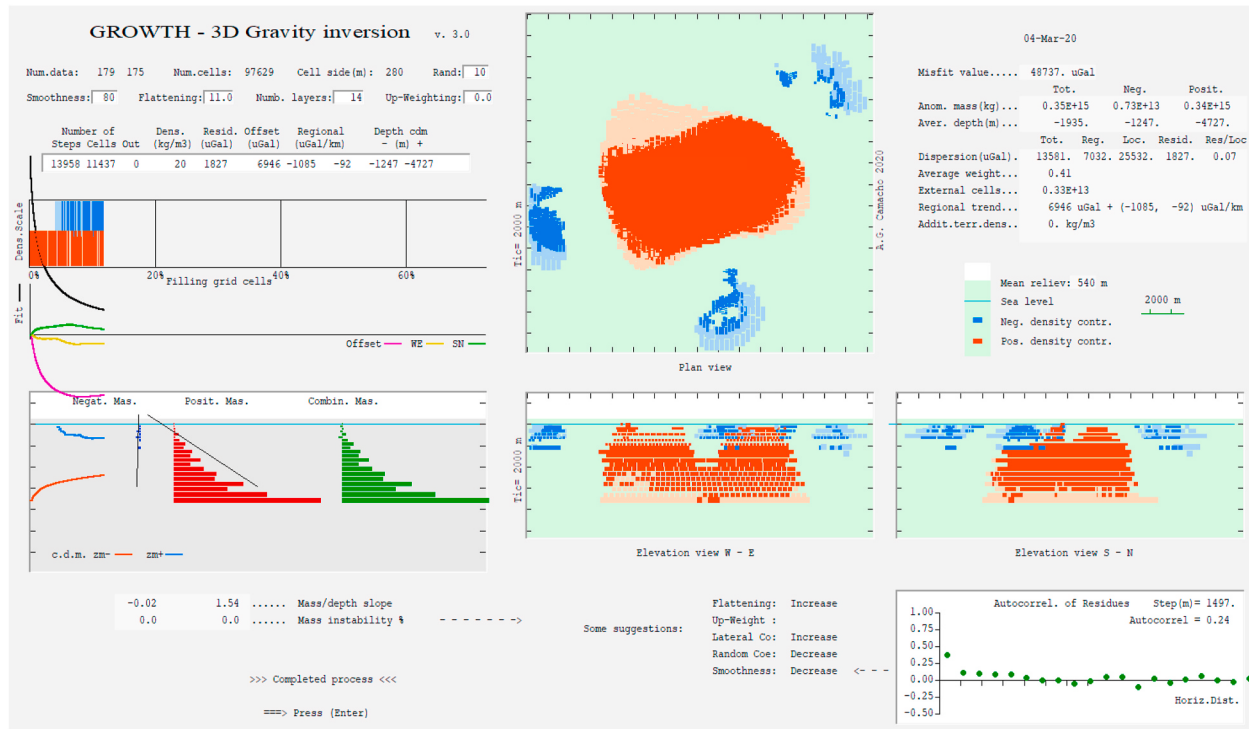


Fig. 2. Example of the graphic display of the intermediate results obtained during the inversion process.

$$\begin{pmatrix} \Delta\rho_j^- \\ \Delta\rho_j^+ \end{pmatrix} = \begin{pmatrix} -1 + \theta_j \\ +1 + \theta_j \end{pmatrix} \varphi_k f, \quad (6)$$

where $f \geq 1$ is the scale factor which relates a basic density variation near to the unity value (positive or negative) with the value finally considered as suitable (the same scale factor as in equation (2)). The software adjusts this scale factor for each step in the growth process fulfilling the minimization conditions. Parameter $\theta_j \geq 0$ allows a continuous density increment to be included in the medium with depth at the j -th cell described by:

$$\rho_j = C \exp(z_j - z_T) \quad (7)$$

where z_T is the depth value for the top surface of the model, usually the topographical level; $C \geq 0$ is a flattening coefficient set at an a priori value that regulates the greater or lesser intensity of exponential variation. The appropriate values for this parameter can be selected by inspecting the results, seeking a reasonable geometric distribution of anomalous bodies that - where possible - avoids high-density anomalous 3D structures overlying others with small density values or vice versa. C

= 0 corresponds to the case of considering a homogeneous medium as the background. Fig. 3 shows some vertical distribution patterns of anomalous, positive and negative masses versus depth, for $C = 0$ (homogeneous background medium), and for $C > 0$ (background medium with an increasing downward density). The software provides these types of graphics to help users make decisions when selecting the flattening coefficient value for suitable modelling.

$\varphi_k \geq 1$ is another factor that allows a lateral attenuation during the growth process. For the k -th step ($k = 1, 2, \dots$), it is given by a function of k :

$$\varphi_k = 1 - (D k)^2 \quad (8)$$

where $D \geq 0$ is a coefficient set to an a priori value. When $D = 0$, we obtain homogeneous 3D anomalous structures with strong density contrast at their edges. When considering a value for $D \gg 0$, the boundaries of the 3D bodies appear more diffused, showing a gradual variation of density from the anomalous body to the background medium. This equation (8) imposes a blurred or abrupt transition at the borders of the anomalous source.

Both approaches, (ii) as default option and (i) by activating option

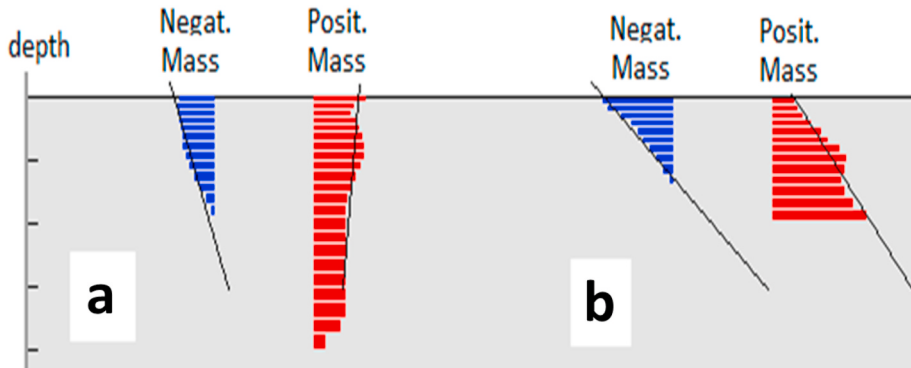


Fig. 3. Effect of the flattening term C (for the downward density increase of the background medium) in the entire vertical distribution of anomalous negative (blue and on the left) and positive (red and on the right) masses. The black line points out the slope of the vertical mass distribution. Panel (a) shows the case $C = 0$, in which the black lines have a slight slope and there is no clear downward density increase. Panel (b) shows the case $C > 0$, in which the black lines are more steeply sloping. Positive mass increases downwards and negative mass decrease downwards. (For interpretation of the references to colour in this figure legend, the reader is referred to the Web version of this article.)

"Sub-horiz. discont" (Fig. 1), are implemented in the new version of the software. For parameters involved in both options, the software offers default values for a general application. An expert user could try more personal values on the results. Option (i) initially appears to be able to provide more realistic models, but also requires more information or more hypotheses to be proposed. The following application example shows the results obtained for both kinds of models.

4. Software package description and its running

Here we present some additional details on the software package and its operation.

The software package consists of two codes:

- ✓ **GROWTH**, which performs the inversion routine and obtains the 3D anomalous density model, and
- ✓ **VIEW**, which allows the users to create the graphical presentation of the original data, the anomalous 3D density distribution obtained, and the residuals among observed and computed gravity anomalies.

The main input file is labelled **GRA.DAT**, and contains the coordinates of the gravity stations and the observed anomaly (see available User Manual in the file **UserManual-GROWTH.TXT**).

The method aims to determine the geometry of an undefined number of anomalous bodies described by aggregating thousands of small rectangular prisms filled with values of anomalous density. To achieve this objective, a 3D grid of regular cells is first determined to represent the subsurface volume. This initial phase of the **GROWTH** code involves

selecting several parameters for geometrical configuration. The inversion method then requires the input of certain values (by means of dialogue windows, with default values). The program works automatically to fill in some of these small prismatic cells, with the possible density contrast to reproduce the anomalous structures.

The following is a list of main values or options that the user must enter or decide:

- a) The side of the modelling cells. We suggest the default values as the best option.
- b) The positive and negative density contrast. The default option is the automatic determination.
- c) The λ value for the fitting-smoothing balance. There is a default value available. The user can try several values and select one, aiming to minimize the autocorrelation of residuals (see bottom-right square in Fig. 2) after displaying the model.
- d) The user must choose between the model as a homogeneous medium or a medium with a downward density increase. The second option is the default. There are three options for the downward density increase: continuous increase, increase according to a large number of regularly spaced layers (default option), and increase according to a small number of layers fully specified by the user.
- e) The user must choose between calculating an automatic determination of the (linear) regional trend (default option) or inputting previously determined fixed values.

There are also some minor parameters (for instance the random coefficient for faster or slower exploration), for which the default value is

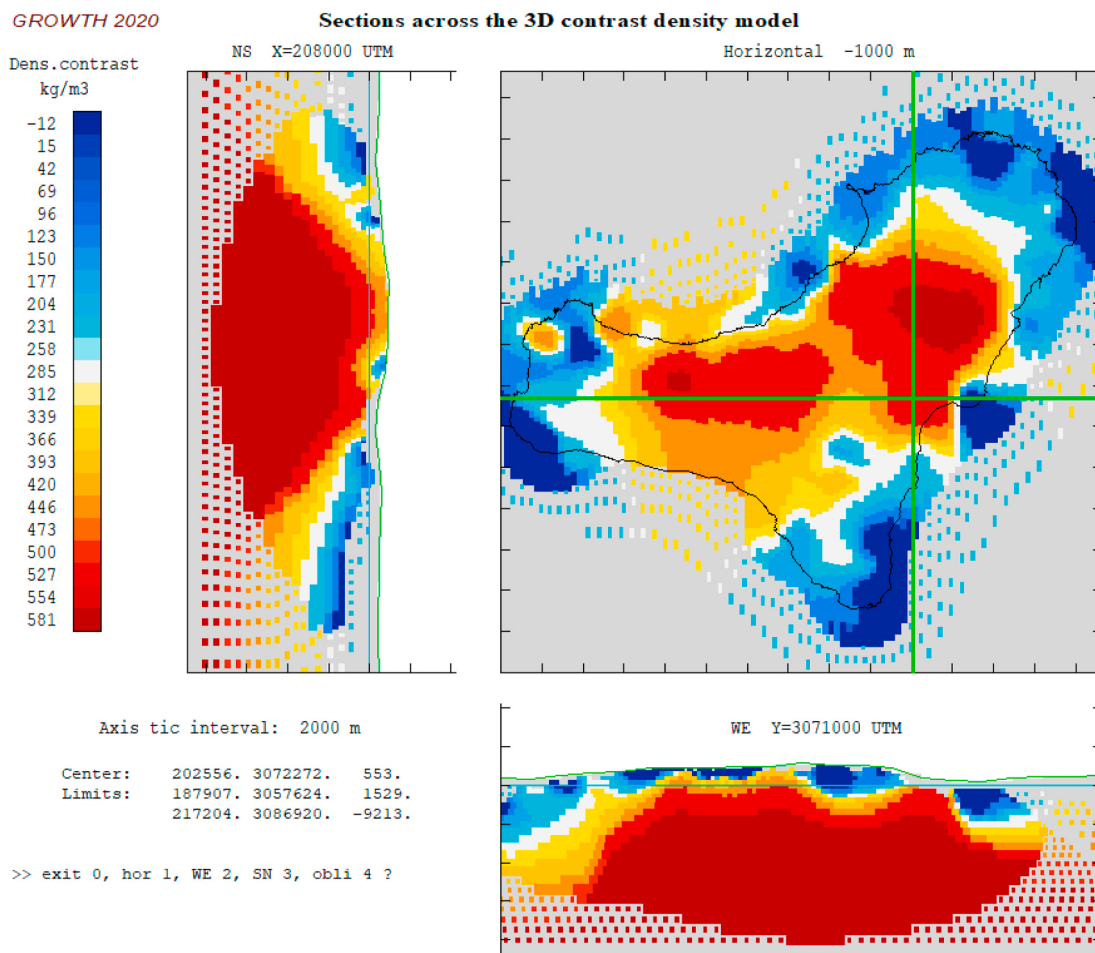


Fig. 4. Example of the graphical representation of the model results produced by the **VIEW** program. It offers views of three sections: horizontal, WE and NS sections of the resulting 3D model for anomalous density distribution below the surface of El Hierro island.

adequate.

The resulting model is exported to an output ASCII file denoted **MOD.DAT**, which includes the adjusted values for every cell, and a final report showing the values used and the resulting characteristic values of the model. A second ASCII file, **FIL.DAT**, collects the observed, regional, local, modelled and residual values for each station. Both files are the input for the **VIEW** program, which creates a graphical representation of the data values and of the resulting model for the subsurface distribution of the anomalous densities (see Fig. 4).

The software package (freely available at github.com and <http://digital.csic.es/>), includes:

- ✓ An introductory file **Readme-GROWTH.TXT**
- ✓ A user manual file, **UserManual-GROWTH.TXT**, giving suggestions and tips for running the software and choosing suitable values for the inversion parameters.
- ✓ The executable codes, **GROWTH.EXE** and **VIEW.EXE**.
- ✓ The files corresponding to a sample application: **GRA.DAT**, **MAP.BLN**, **MOD.DAT**, **FIL.DAT**.

The application case included in the files available on our website corresponds to a real study case: the volcanic island of El Hierro (Canary Islands). It is described in the following section.

5. Application example: the volcanic island of El Hierro

In view of the importance of knowing the crustal structure in volcanic areas, as previously described, we have chosen the study of the crustal structure of El Hierro, Canary Islands, as a test case for the application of this new methodology.

In this test case we use the non-subjective inversion upgraded software package **GROWTH 3.0** to analyse new and recently observed terrestrial gravity data on El Hierro island to obtain a structural model of the subsurface mass below its surface. A discussion on the geological and volcanological interpretation of the structural results is provided below.

5.1. Geological setting

The Canary Islands consist of seven major Islands located close to the northwest African margin. The Island of El Hierro is at the southwesternmost extreme of the Canary Islands volcanic archipelago, at 27.7° north and 18.0° west, and is the youngest and, at 278.5 km², the smallest island in the archipelago. El Hierro (Fig. 5) is a small basaltic oceanic island volcano with maximum altitudes of 1500 m, rising about 5500 m from its base in 4000 m of water. The oldest subaerial rocks have been dated at 1.12 ± 0.02 Ma (Guillou et al., 1996), although much of El Hierro is covered by more recent lavas that serve as a record of its rapid

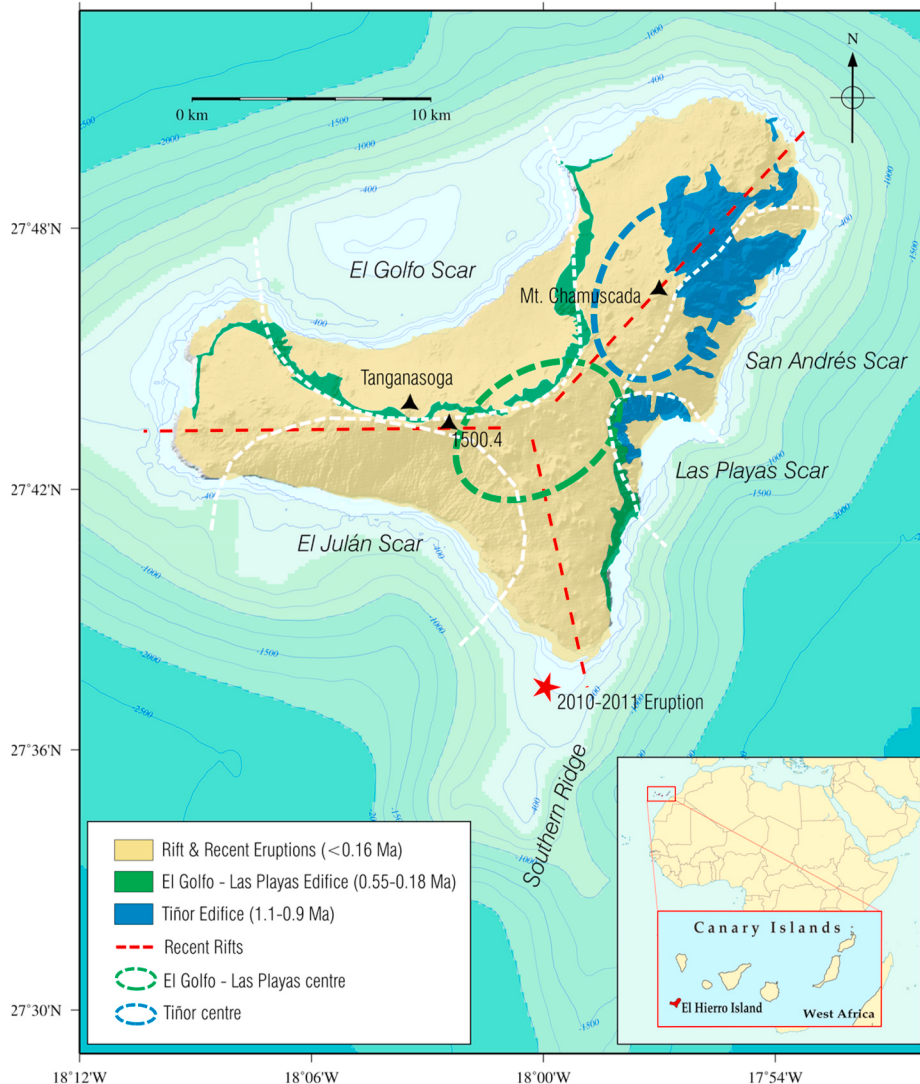


Fig. 5. Location of El Hierro, and simplified geological map after Ancochea et al. (2004) with the location of the centres of the volcanic edifices, recent rifts and the collapsed escarpments.

growth.

The Island is triangular in shape, with elevated bisections that converge in the centre to form a plateau about 1000 m above sea level (m asl). These bisections correspond to rifts which concentrate most of the island's recent volcanic activity (Pellicer, 1977; Fúster et al., 1993), of which the two most developed rifts are the NE and the SSE. Semi-circular depressions corresponding to collapse escarpments have opened between these rifts (Fig. 5): El Golfo in the N, El Julán in the SW and Las Playas in the ESE (Holcom and Searle, 1991; Masson, 1996; Urgeles et al., 1997; Masson et al., 2002).

In addition to sub-aerial volcanism, bathymetric studies (Gee et al., 2001) have revealed a significant number of well-preserved volcanic cones on the submarine flanks of the island, specifically on the continuation of the rifts, suggesting that significant submarine volcanic activity has occurred recently. The latest submarine eruption took place between October 2011 and February 2012 in the southern rift zone, about 2 km offshore (González et al., 2013; Martí et al., 2013; Aparicio and Solana, 2015). This recent activity makes El Hierro an interesting zone for updating previously computed crustal models (Montesinos et al., 2006; Gorbatikov et al., 2013; Sainz-Maza et al., 2017) using this upgraded software package.

The island of El Hierro is characterized by three main periods of volcanic activity: (1) the Tiñor edifice (1.12–0.88 Ma), (2) El Golfo-Las Playas edifice (545–176 ka), and (3) Dorsal volcanism (158 ka –Present time) (Fúster et al., 1993; Balcells et al., 1997; Carracedo et al., 2001).

Subaerial volcanic activity began in El Hierro with the development of the Tiñor volcano on the NE flank of the Island with the emission of typical massive basalts (Fúster et al., 1993). The volcano developed rapidly, showing several growth stages and culminating in a final explosive stage, and was a probable precursor of the NW flank of the collapsed edifice which occurred about 882 ka ago (Balcells et al., 1997; Carracedo et al., 2001). This volcanic edifice standing over 1000 m high did not occupy the entire current island of El Hierro, only its E and NE part (Fig. 6a).

Considering the tilt of the lava flows, the situation of the highest outcrops and the convergence zone of the dykes, which follow a broadly radial pattern, it can be deduced that the centre of this volcanic edifice was located to the N of Las Playas and E from El Golfo (Fig. 5). After an interruption of about 300 ka, a new volcano was formed (El Golfo-Las Playas) between approximately 545 ka to 176 ka. This new volcanic edifice was essentially basaltic with some trachybasalts and trachytes. It was much larger, covering most of the Tiñor edifice, totally filling the depression formed by the lateral collapse, and extending over most of what is now the island (Fúster et al., 1993; Balcells et al., 1997; Carracedo et al., 2001) (see Fig. 6b). Following the same criteria as in the Tiñor edifice, it can be surmised that the centre of the volcano must have been located in the central area of the island (Fig. 5). The excessive growth of this volcano triggered the failure of its northern flank and generated the spectacular scarp and present El Golfo depression (Fig. 6c).

Subsequent volcanism included emission vents arranged in a three-armed rift system (rift volcanism), predominantly basic-tephritic, with ages ranging from 145 ka to prehistoric times and converging in an area similar to the centre of the El Golfo-Las Playas edifice. This last phase of volcanic activity, of much smaller temporal and volumetric scale than the previous ones, masks most of the previous structure of the island [Fig. 6c, Fúster et al. (1993) and Becerril et al. (2015)].

5.2. Gravity inversion modelling

Gravity studies in volcanic areas are particularly interesting and can provide valuable insights into shallow sub-surface density anomalies associated with the structural and magmatic history of a volcanic system (see some references above, in Introduction). For example, rift zones and underlying dyke swarms occur in most volcanoes, and contain the paths taken by magmas moving through the crust (Walker, 1999). These

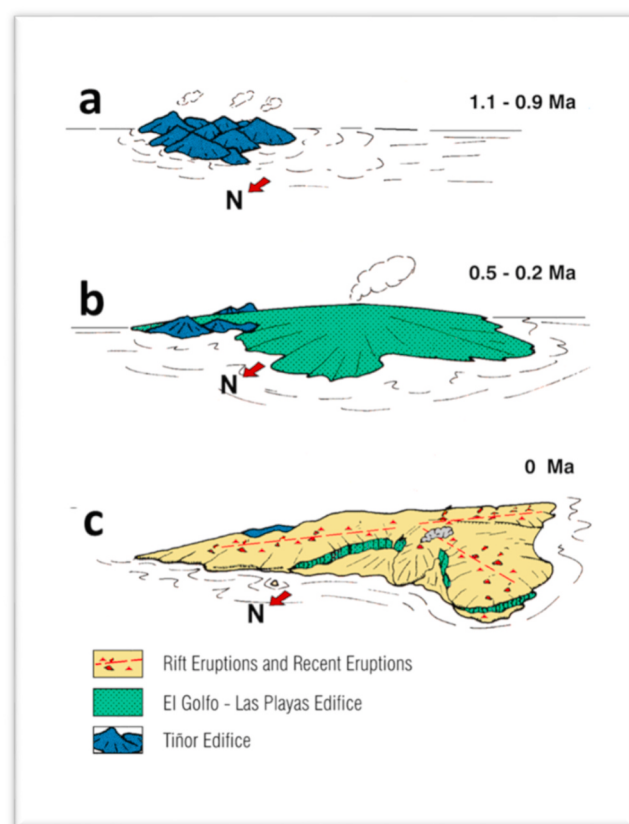


Fig. 6. Simplified diagram of the formation of subaerial part of the island of El Hierro (based on Fúster et al., 1993). See main text for explanation of panels a, b and c.

intrusive complexes are normally positioned and oriented by tectonic structures, or propagate laterally from volcanic centres along rift zones at neutral buoyancy levels. Swarms of dykes and sills close to the surface represent conduits for magma transport from the reservoirs to the surface or to shallow intrusions. The intrusion of dykes may also cause the bending or initiation of a rift zone. Complexes of intrusions and cumulates beneath the volcano develop upwards during its growth (Ryan, 1987), causing the centre of the mature oceanic shield volcano to appear as a high-density column-like body. This produces measurable gravity anomalies that can be detected and modelled using an inversion methodology. Positive anomalies characterize normally basaltic volcanoes, and are caused by a dense intrusive complex/magma body, which respect to its surroundings (Rymer and Brown, 1986). Negative anomalies can be due to erupted highly silicic pyroclastic ash and pumice or also to uncompacted caldera infill, with possible contributions from low-density magma bodies.

With these approaches, the areas of positive gravimetric anomalies could be expected to be found close to the centres of large volcanic edifices where most of the intrusions are located and the density of dikes is greater. In the case of El Hierro, these positive anomalies could in some way mark the position of the centres of the Tiñor and El Golfo-Las Playas edifices, and even the rifts (Fig. 5). However, it should be noted that only subaerial volcanic activity can be observed on the surface and as over 90% of the volume of the island is underwater (Schmincke, 1976), gravimetric anomalies will also be affected – possibly even significantly – by possible ancient underwater volcanic complexes. This is one reason why gravimetric anomalies and subaerial volcanic edifices do not always coincide, as occurs for example in Lanzarote (Camacho et al., 2019).

5.3. Gravity survey and Bouguer anomaly

The gravity field observation was carried out from June 30-July 7, 2014, and 179 data points were obtained (Fig. 7a). GNSS (Global Navigation Satellite System) observations were made simultaneously with the gravimetric observations.

The main purpose of these GNSS observations was to guarantee centimetre precision in horizontal and vertical positioning at the measured gravity points. This was done by means of two TOPCON HiperPro (GPS + GLONASS) dual frequency receivers with built-in geodetic antenna. The method generally used when there was sufficient communications coverage was the Real Time Kinematic (RTK) phase difference, relying on the GRAFCAN RTK network (<https://www.grafcan.es/red-de-estaciones>). The phase difference fast-static differential method (Hoffmann-Wellenhof et al., 2008) was used for the rest of the gravity points. The data recorded with the GNSS receivers were subsequently processed with the Leica Infinity software (<https://leica-geosystems.com/en-gb/products/gnss-systems/software/leica-infinity>) in two stages. In a first stage, the points observed by fast-static were computed with the GRAFCAN Continuously Operating Reference Stations network, using precise ephemeris and the CODE global ionospheric model (Dach et al., 2019), and NGS absolute antenna center calibrations (Mader and Bilich, 2012). Ambiguities were fixed using L3 free ionosphere combination solutions with the VMF tropospheric model (Boehm and Schuh, 2004). The RTK vectors of the remaining gravity points were integrated in a second process. The geoid undulations from the EGM08-REDNAP model (IGN, 2010) were included in order to obtain orthometric altitudes. We estimate an uncertainty of better than ± 5 cm for the resulting positions.

The gravity data were reduced following the usual steps for correcting observations (Groten, 1980): (1) tidal correction, (2) global traverse fit (with an estimated root mean square residual of $35 \mu\text{Gal}$, and adjusting a value $593 \pm 30 \mu\text{Gal}/\text{day}$ for instrumental drift for Scintrex CG5); (3) normal gravity for ellipsoid; (4) elevation effect; (5) Bouguer sheet; and (6) terrain correction (up to 60 km) (using an estimated average terrain density value of 2350 kg/m^3 , estimated automatically by the program). MacFarlane and Ridley (1968) used a terrain density value of 2400 kg/m^3 for Tenerife; and Bosshard and MacFarlane (1970) used 2300 kg/m^3 for the western Canary Islands. Both are very similar to the value we used, and the estimated accuracy for the gravity observation was $\pm 35 \mu\text{Gal}$ (according to the traverse fit). Fig. 7b show a map for the relative Bouguer anomaly values.

5.4. Gravity inversion results

We provide this test case to enhance the understanding of the possibilities of the **GROWTH 3.0** inversion approach. We present the results obtained using the two different approaches for the same gravity anomaly data set determined for El Hierro from the gravity observations, corresponding to modelling options (i) and (ii), described in Section #2.

We start by obtaining a model for anomalous density distribution from the gravity anomaly data as a structure of sub-horizontal layers (case i of downward increase for background medium). We apply the present **GROWTH 3.0** package with the gravity anomaly data in the **GRA.DAT** file according to the appropriate format. We then begin running the code, and accept all default names and values except the following ones: for the 3D grid, we select 280 as “Mean length (m) for cells” (instead of the default value 414). This produces an acceptable grid with 97629 cells (smaller than the limit of 99000), and allows for higher resolution (smaller cell size). We then select 70 as “Balance fact. Mass-fitness” (the λ value) (which gives a nearly null auto-correlation value for the resulting residual values). We select “Sub-horiz. discount.” to obtain a model as sub-horizontal layers (approach i). A new dialogue window appears, in which we select 10 layers (for instance) and a flatness value (a^+, a^- above) out of 10 (selected after trying various options). The process then runs automatically after this step, including free adjustment of the lineal regional trend and density contrast values.

The resulting 3D density model is written in the **MOD.DAT** file. It can be plotted (observed, modelled and residual values) with the **VIEW.FOR** code. Figs. 8 and 9 shows some views of the model obtained in this way for El Hierro.

For comparison, we now show another anomalous density model but obtained through the modelling approach (ii) for a general downward density increase. In this case we use the same 3D grid with an average cells size of 280 m, but assume a continuous downward density increase by setting the “Flattening coef” close to zero, $C = 0.2$ for instance. We also assume a lateral smoothing of $D = 10$. The density contrast and regional trend are again freely adjusted, and the default values are assumed for the remaining parameters and options. This approach produces the model shown in Fig. 10, with isolated bodies within a medium with a continuous increment of density with depth.

Figs. 8–10, corresponding to both modelling approaches (i) and (ii), show that approach (i) produces model results with a generally more realistic appearance (layered structures). However, although it may be less realistic, model (ii) in Fig. 10 identifies certain patterns in the

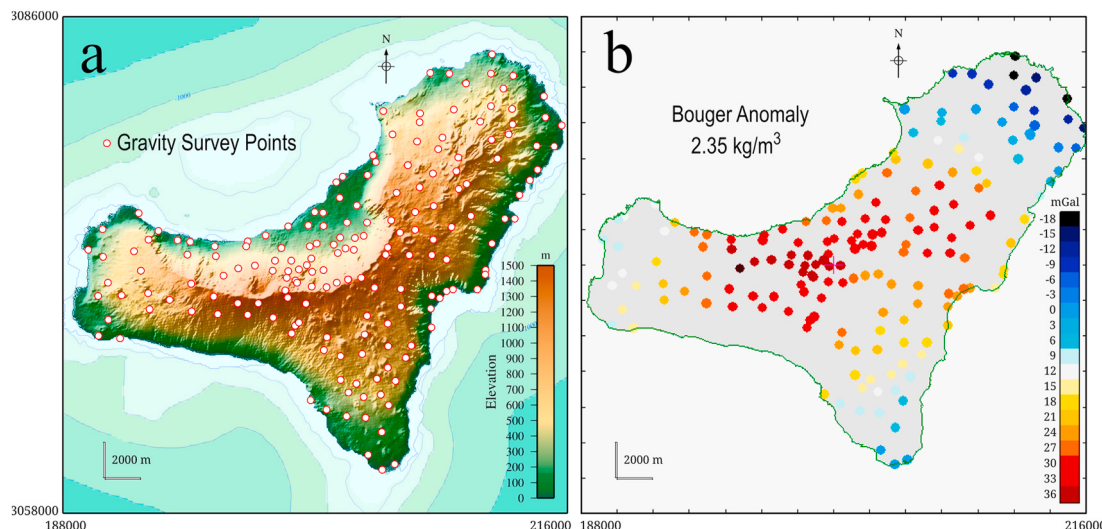


Fig. 7. (a) El Hierro. Digital Elevation model and geographic location of the 179 gravity observation points. (b) Relative Bouguer gravity anomaly (mGal) for an average terrain density value 2.35 kg/m^3 .

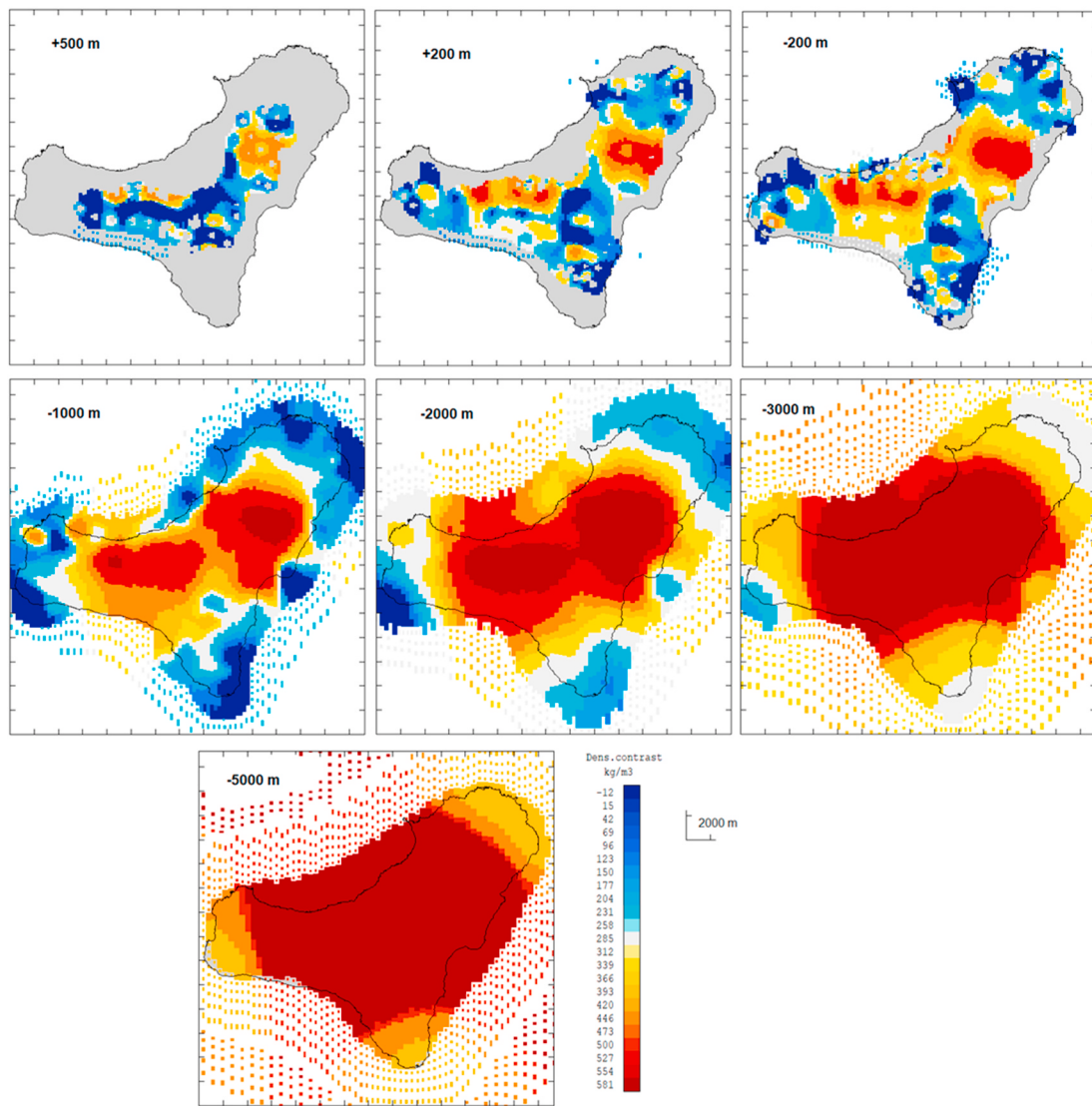


Fig. 8. Several horizontal sections (for depths of 500 and 200 m above sea level (m asl) and 200, 1000, 2000, 3000 and 6000 m bsl) of the resulting 3D density structure distribution modelled for El Hierro. Red shades indicate high density and blue shades indicate low-density anomalies respectively. (For interpretation of the references to colour in this figure legend, the reader is referred to the Web version of this article.)

anomalous source structure which would be difficult to detect (or would appear more diluted) in the first kind of model shown in Figs. 8 and 9.

5.5. Discussion of results and volcanological interpretation

From the 3D models above, we can propose some geological and volcanological interpretations of the general assumption that high density bodies correspond to ancient cooled magma conduits, magma chambers and dyke swarms.

- (1) As in the case of the other Islands in the Canaries, deep magmatism would not be disseminated below the entire island, but concentrated in some reduced genetic regions (see the panels in Fig. 8 for depths of -200 m, -1000 m and -2000 m depth).
- (2) At depths of less than 1–2 km, (see Figs. 8–10), we observe that the positive anomaly corresponding to the intrusive body of El Hierro has a branched appearance. Above that depth, the main body can be seen to comprise two nearly independent branches. This is a curious peculiarity. For instance, the neighbouring island of La Palma is fully monogenetic from bottom to the top (Camacho et al., 2009; Prieto et al., 2009), with a single branch.

- (3) Both branches appear to include a top plateau level with some minor sub-branches in very shallow positions. However, the plateau level for the western branch is at a depth of about 2000 m below sea level (m bsl) (Fig. 8, WE profiles), and the plateau level for the eastern branch is at a depth of 1500 m bsl (Fig. 8, NS profiles). We also suggest some levels for branching: a deeper level of 4.5 km depth for the main division and 2 km depth for the secondary branch. For example, González et al. (2013) found a level of magma stagnation at El Hierro at ~4.5 km, on the paleo-oceanic seafloor during the unrest previous to the submarine eruption that took place between 10 October 2011 and end of February 2012 in the southern rift zone, 2 km off the coast (Fig. 5). The 2 km magmatic level is also present in other volcanic islands. In Gran Canaria, estimated pressure in fluid indicate reservoirs at a depth of 2–4 km, which can be interpreted as a relevant horizon of neutral buoyancy (Hansteen et al., 1998)). A magma storage depth was inferred in Tenerife at about 2 ± 1 km bsl (Andújar et al., 2010); active magmatic chambers have been detected in La Piton de la Fournaise, at ~2.5 km depth (Peltier et al., 2009); the Fernandina Island volcano has two levels of magma storage at depths of ~1 and ~5 km (Chadwick et al.,

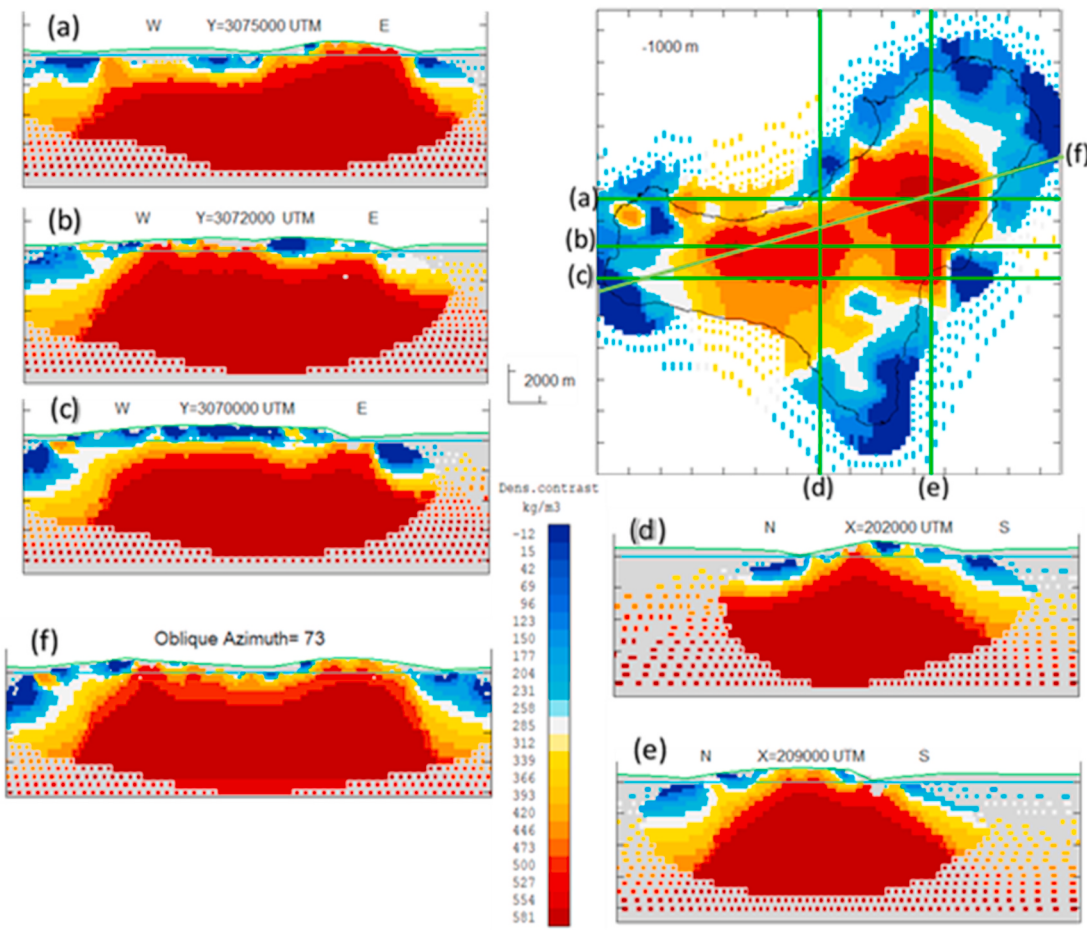


Fig. 9. Several vertical WE (a, b, and c) and NS (d and e) sections of the resulting 3D modelling of the density structure. The location of WE and SN sections are indicated (green lines) on the horizontal section for a depth of 1000 m bsl. (For interpretation of the references to colour in this figure legend, the reader is referred to the Web version of this article.)

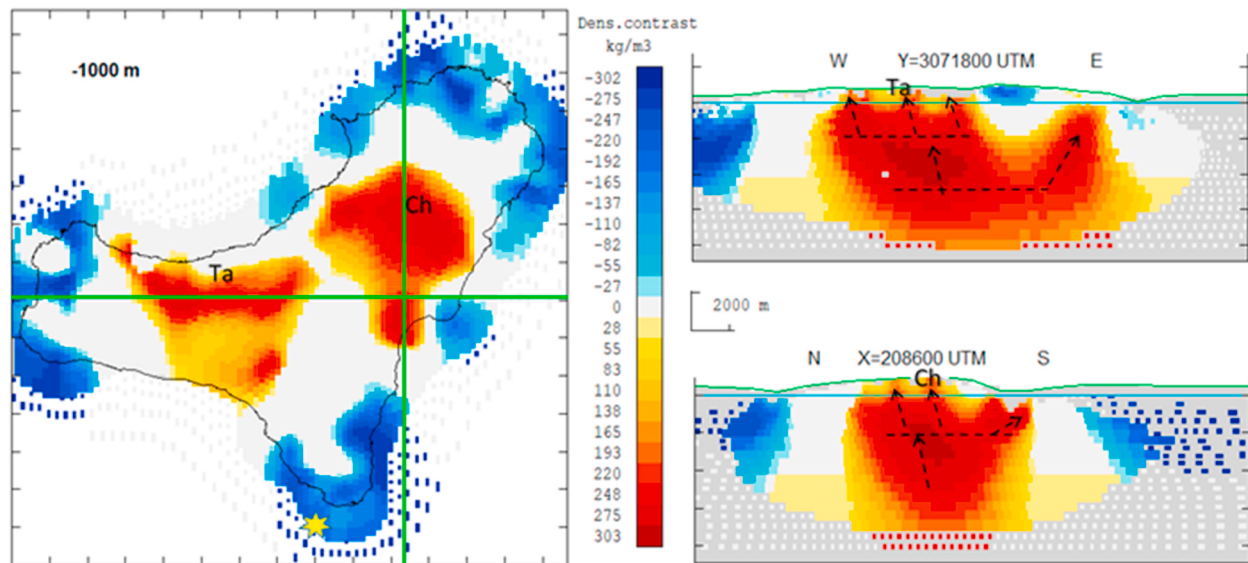


Fig. 10. Horizontal section at 1000 m bsl, and vertical WE and NS vertical profiles of the resulting 3D model for the case of a surrounding medium with a slight continuous increase in density downwards. The dashed lines indicate the locations of two dated eruptions: Ta [Tanganasoga volcano (4000 yr BP)], Ch [Mount Churruasca (2500 yr BP)]. The yellow star indicates the location of the 2011 eruption in a peripheral low-density area. (For interpretation of the references to colour in this figure legend, the reader is referred to the Web version of this article.)

- 2011); Bagnardi and Amelung, 2012), which may correspond to unerupted stagnated magma which later solidified.
- (4) We propose to associate each sub-branch with major growth episodes on the Island. For these volcanic structures, the magma would ascend from deep sources following an almost vertical path. The two positive intrusive bodies (or sub-branches), are located in the position occupied by the centres of the volcanic edifices of Tiñor and El Golfo-Las Playas, and therefore denote the areas with maximum concentration of intrusive dikes at 1.1–0.9 Ma and 0.5–0.2 Ma respectively (Figs. 5 and 8).
- (5) The 3D density model shows that the structural configuration, controlled by a three-armed rift zone system that characterizes the recent volcanic activity of the island, does not continue at depth. This structure would not therefore have led to the formation of large landslides, as suggested by other authors (see e.g., Carracedo, 1994). The deep structure of the island is an elongated body in the NE-SW or ENE-WSW direction (Figs. 8 and 9), which can be interpreted as the result of the union of the two great volcanic edifices of Tiñor and El Golfo – Las Playas. These edifices succeeded each other over time, so the volcanic activity must have migrated in that direction at an average speed of between 1 and 2 cm/year.
- (6) Subsequent volcanism from emission vents arranged in a three-armed rift system (rift volcanism). We observe that extreme areas of the three-rift system are characterized by low density structures (Fig. 8), which facilitates the behaviour of the plumbing magmatic system described by González et al. (2013) in the case of the 2011–2012 El Hierro eruption.

As is the case in many inversion approaches, the different zones of the resulting inverse model (Figs. 8–10) do not have the same relative confidence due to the fact that the gravimetric sensitivity (for instance, sensitivity to the mass in kg/μGal) between the whole survey network and the model cells depend on their relative distance and position. Cells located in deep or peripheral areas of the model will have a smaller relative confidence than those located just below the survey network at depths between 0 and 6 km. For instance, in Figs. 8–10 we have drawn with continuous painting the acceptable regions (according an arbitrary sensitivity limit of 20×10^9 kg/μGal) and with discontinuous painting the very low confidence zones and details.

6. Conclusions

The new upgraded and freely available software package **GROWTH 3.0** allows for a more flexible and realistic inversion of gravity anomaly data to obtain positive and negative anomalous 3D density structures with a free geometry and merged in media with general downward density increase. Sub-horizontal layered structures and isolated bodies can also be adjusted. The new version is operationally simpler (one computing code and one graphic code) and provides default values for all the parameters, and runs on the current Microsoft Windows 10 operating system. Some relevant aspects are:

- An almost automatic approach in an easy and user-friendly context, with dialogue windows that include suitable default values and options and graphic outputs. It is fast to run (a few minutes, depending on the number of data points).
- Determination of density contrast, free 3D geometry of the anomalous structures, linear regional trend, and correction to terrain density.
- Several modelling options to take account of a general downward density increase or a layered medium.

The results for the test case of El Hierro in the Canary Islands show the type of results and conclusions that can be achieved from the use of the **GROWTH 3.0** package.

Future work will be carried out in order to improve the inversion methodology to allow its application in a range going from very small scales (few hundred square meters) to regional scales (thousands of square km) seeking an increase in its applicability.

Authorship Statement

AGC had the original idea of this study, AGC and JF organized and coordinated the work. AGC and JF wrote the manuscript with the participation of all the rest of co-authors. AGC wrote the code with support from JF. JF coordinated the research project which supported this work. JFP, AGC and AA carried out the gravimetric and GNSS fieldwork on the island of El Hierro. EA coordinated, with the support of AA, the geological and volcanological interpretation of the structural results of applying the software package to El Hierro, Canary Islands.

Computer code availability

The **GROWTH 3.0** software package described here, developed by Antonio G. Camacho with support from Jose Fernández (Instituto de Geociencias, CSIC-UCM. Calle del Doctor Severo Ochoa, nº 7. Ciudad Universitaria. 28040-Madrid. Phone: +34-913944632, e-mails: antonio.camacho@mat.ucm.es, jft@mat.ucm.es), the source codes, user manual, executable files and a test example (including input data and results) can be freely downloaded from the repository at https://github.com/josefern/GROWTH_3.0_software, from digital.csic.es or requested from the corresponding author, under an open source license. The software is written in FORTRAN and is compatible with the current Microsoft operating system, Windows 10 Pro. The software has been compiled using Intel® Visual Fortran Compiler, with a Quickwin application project. The complete compilation requires several additional files (codes, auxiliary files for compilation, etc.), which are also freely available on the website. All the files have a size of 11.5 Mb.

Data availability

Datasets related to this article can also be found at https://github.com/josefern/GROWTH_3.0_software, together with the software.

Declaration of competing interest

The authors declare that they have no known competing financial interests that could have appeared to influence the work reported in this paper.

Acknowledgments

This research was mainly funded by the Spanish Ministerio de Ciencia, Innovación y Universidades research project DEEP-MAPS, grant agreement number RTI2018-093874-B-100, and also partially by the Spanish Ministerio de Ciencia e Innovación research projects AYA2010-17448, AQUARISK, CGL2017-86241-R and the Spanish National Research Council (CSIC) project 201530E019. We thank the Editor-in-chief D. Grana, one anonymous reviewer and V. C. F. Barbosa which help us, with their comments and suggestions, to improve the quality of this work.

References

- Ancochea, E., Barrera, J.L., Bellido, F., Benito, R., Brändle, J.L., Cebriá, J.M., Coello, J., Cubas, C.R., De la Nuez, J., Gómez, J.A., Hernán, F., Herrera, R., Huertas, M.J., López-Ruiz, J., Martí, J., Muñoz, M., Sagredo, J., 2004. Canarias y el vulcanismo neógeno peninsular. *Geología de España*. SGE-IGME, Madrid, pp. 634–680.
- Andújar, J., Costa, F., Martí, J., 2010. Magma storage conditions of the last eruption of Teide volcano (Canary Islands, Spain). *Bull. Volcanol.* 72, 381–395. <https://doi.org/10.1007/s00445-009-0325-3>.

- Aparicio, A., Solana, C., 2015. Las rocas de la erupción del Hierro (Islas Canarias). Octubre-Diciembre 2011, vol. 109. Boletín de la Real Sociedad Española de Historia Natural, Sección de Geología, pp. 37–42 ([in Spanish]).
- Bagnardi, M., Amelung, F., 2012. Space-geodetic evidence for multiple magma reservoirs and subvolcanic lateral intrusions at Fernandina Volcano, Galápagos Islands. *J. Geophys. Res.* 117, B10406. <https://doi.org/10.1029/2012JB009465>.
- Balcells, R., Gómez, J.A., 1997. Memorias y mapas geológicos del Plan MAGNA a escala 1:25000 de las hojas correspondientes a la isla de El Hierro. Hojas de: Valverde, Sabinosa, Tigaday, Taibique y La Restinga. IGME, Madrid, Spain [in Spanish].
- Barbosa, V.C.F., Silva, J.B.C., 1994. Generalized compact gravity inversion. *Geophysics* 59, 57–68.
- Becerril, L., Galindo, I., Martí, J., Gudmundsson, A., 2015. Three-armed rifts or masked radial pattern of eruptive fissures? The intriguing case of El Hierro volcano (Canary Islands). *Tectonophysics* 647–648, 33–47. <https://doi.org/10.1016/j.tecto.2015.02.006>.
- Bertete-Aguirre, H., Cherkaev, E., Oristaglio, M., 2002. Non-smooth gravity problem with total variation penalization functional. *Geophys. J. Int.* 149, 499–507. <https://doi.org/10.1046/j.1365-246X.2002>.
- Boehm, J., Schuh, H., 2004. Vienna mapping functions in VLBI analyses. *Geophys. Res. Lett.* 31, L101603. <https://doi.org/10.1029/2003GL018984>.
- Bosschart, E., MacFarlane, D.J., 1970. Crustal structure of the western canary islands from seismic refraction and gravity data. *J. Geophys. Res.* 75, 4901–4917. <https://doi.org/10.1029/JB075i026p04901>.
- Boulanger, O., Chouteau, M., 2001. Constraints in 3D gravity inversion. *Geophys. Prospect.* 49, 265–280.
- Camacho, A.G., Montesinos, F.G., Vieira, R., 2000. Gravity inversion by means of growing bodies. *Geophysics* 65 (1), 95–101. <https://doi.org/10.1190/1.1444729>.
- Camacho, A.G., Montesinos, F.G., Vieira, R., 2002. A 3-D gravity inversion tool based on exploration of model possibilities. *Comput. Geosci.* 28 (2), 191–204. [https://doi.org/10.1016/S0098-3004\(01\)00039-5](https://doi.org/10.1016/S0098-3004(01)00039-5).
- Camacho, A.G., Nunes, J.C., Ortiz, E., França, Z., Vieira, R., 2007. Gravimetric determination of an intrusive complex under the island of Faial (Azores). Some methodological improvements. *Geophys. J. Int.* 171 (1), 478–494. <https://doi.org/10.1111/j.1365-246X.2007.03539.x>.
- Camacho, A.G., Fernández, J., González, P.J., Rundle, J.B., Prieto, J.G., Arjona, A., 2009. Structural results for La Palma Island using 3-D gravity inversion. *J. Geophys. Res.* 114, B05411. <https://doi.org/10.1029/2008JB005628>.
- Camacho, A.G., Fernández, J., Gottsmann, J., 2011a. The 3-D gravity inversion package GROWTH2.0 and its application to Tenerife Island, Spain. *Comput. Geosci.* 37 (4), 621–633. <https://doi.org/10.1016/j.cageo.2010.12.003>.
- Camacho, A.G., Fernández, J., Gottsmann, J., 2011b. A new gravity inversion method for multiple sub-horizontal discontinuity interfaces and shallow basins. *J. Geophys. Res.* 116, B02413. <https://doi.org/10.1029/2010JB008023>.
- Camacho, A.G., Carmona, E., García-Jerez, A., Sánchez-Martos, F., Prieto, J.F., Fernández, J., Luzón, F., 2015. Structure of alluvial valleys from 3-D gravity inversion: the Low Andarax Valley (Almería, Spain) test case. *Pure Appl. Geophys.* 172, 3107–3121. <https://doi.org/10.1007/s00024-014-0914-8>.
- Camacho, A.G., Prieto, J.F., Ancochea, E., Fernández, J., 2019. Deep volcanic morphology below Lanzarote, Canaries, from gravity inversion: new results for Timanfaya and implications. *J. Volcanol. Geoth. Res.* 369, 64–79. <https://doi.org/10.1016/j.jvolgeores.2018.11.013>.
- Carracedo, J.C., 1994. The Canary Islands: an example of structural control on the growth of large oceanic-island volcanoes. *J. Volcanol. Geoth. Res.* 60, 225–241.
- Carracedo, J.C., Rodríguez Badiola, E., Guillou, H.J., de la Nuez, J., Pérez Torrado, F.J., 2001. Geology and volcanology of the western Canaries: La Palma and El Hierro. *Estud. Geol.* 57 (5–6), 171–295. <https://doi.org/10.3989/egeol.01575-6>.
- Chadwick, W.W., Jónsson, S., Geist, D.J., Poland, M., Johnson, D.J., Batt, S., Harpp, K.S., Ruiz, A., 2011. The May 2005 eruption of Fernandina volcano, Galápagos: the first circumferential dike intrusion observed by GPS and InSAR. *Bull. Volcanol.* 73, 679–697. <https://doi.org/10.1007/s00445-010-0433-0>.
- Chávez-García, F.J., Luzón, F., Raptakis, D., Fernández, J., 2007. Shear-wave velocity structure at Teide volcano. Results using microtremors with the SPAC method and implications for interpretation of geodetic results. *Pure Appl. Geophys.* 164/4, 697–720. <https://doi.org/10.1007/s00024-007-0184-9>.
- Chen, Z., Meng, X., Zhang, S., 2015. 3D gravity interface inversion constrained by a few points and its GPU acceleration. *Comput. Geosci.* 84, 20–28. <https://doi.org/10.1016/j.cageo.2015.01.008>.
- Dach, R., Schaer, S., Arnold, D., Prange, L., Sidorov, D., Stebler, P., Villiger, A., Jaeggi, A., 2019. CODE Rapid Product Series for the IGS. Astronomical Institute, University of Bern. <https://doi.org/10.7892/boris.75854.3>. Published by. <http://www.aiub.unibe.ch/download/CODE>.
- Deplus, C., Bonvalot, S., Dahrina, D., Diamant, M., Harjono, H., Dubois, J., 1995. Inner structure of the Krakatau volcanic complex (Indonesia) from gravity and bathymetry data. *J. Volcanol. Geoth. Res.* 64, 23–52.
- Farquharson, C.G., Ash, M.R., Miller, H.G., 2008. Geologically constrained gravity inversion for the Voisey's Bay Ovoid deposit. *Lead. Edge* 27, 64–69.
- Fernández, J., González, P.J., Camacho, A.G., Prieto, J.F., Bru, G., 2015. An overview of geodetic volcano research in the canary islands. *Pure Appl. Geophys.* 172/11, 3189–3228. <https://doi.org/10.1007/s00024-014-0916-6>.
- Fernández, J., Pepe, A., Poland, M.P., Sigmundsson, F., 2017. Volcano Geodesy: recent developments and future challenges. *J. Volcanol. Geoth. Res.* 344, 1–12. <https://doi.org/10.1016/j.jvolgeores.2017.08.006>.
- Fournier, N., Rymer, H., Williams-Jones, G., Brenes, J., 2004. High-resolution gravity survey: investigation of subsurface structures at Poás volcano, Costa Rica. *Geophys. Res. Lett.* 31, L15602. <https://doi.org/10.1029/2004GL020563>.
- Fúster, J.M., Hernán, F., Cendrero, A., Coello, J., Cantagrel, J.M., Ancochea, E., Ibárrula, E., 1993. Geocronología de la isla de El Hierro (Islas Canarias). *Bol. R. Soc. Esp. Hist. Nat.* 88 (1–4), 85–97 ([in Spanish]).
- Gee, M.J.R., Watts, A.B., Masson, D.G., Mitchell, N.C., 2001. Landslides and the evolution of El Hierro in the canary islands. *Mar. Geol.* 177 (3–4), 271–293. [https://doi.org/10.1016/S0025-3227\(01\)00153-0](https://doi.org/10.1016/S0025-3227(01)00153-0).
- Ghalehnoee, M.H., Ansari, A., Ghorbani, A., 2017. Improving compact gravity inversion using new weighting functions. *Geophys. J. Int.* 208, 546–560.
- González, P.J., Samsonov, S.V., Pepe, S., Tiampo, K.F., Tizzani, P., Casu, F., Fernández, J., Camacho, A.G., Sansosti, E., 2013. Magma storage and migration associated with the 2011–2012 El Hierro eruption: implications for crustal magmatic systems at oceanic island volcanoes. *Journal of Geophysical Research, Solid Earth* 118, 4361–4377. <https://doi.org/10.1002/jgrb.50289>.
- Groten, E., 1980. *Geodesy and the Earth's Gravity Field*, vols. I and II. Duemmler Verlag, Bonn, p. 724.
- Gorbatiuk, A.V., Montesinos, F.G., Arnoso, J., Yu Stepanova, M., Benavent, M., Tsukanov, A.A., 2013. New features in the subsurface structure model of El Hierro island (Canaries) from low-frequency Microseismic sounding: an insight into the 2011 seismo-volcanic crisis. *Surv. Geophys.* 34, 463–489. <https://doi.org/10.1007/s10712-013-9240-4>.
- Gottsmann, M.T., Camacho, A.G., Martí, J., Wooller, L., Fernández, J., García, A., Rymer, H., 2008. Shallow structure beneath the Central Volcanic Complex of Tenerife from new gravity data: implications for its evolution and recent reactivation. *Phys. Earth Planet. In.* 168 (3–4), 212–230. <https://doi.org/10.1016/j.pepi.2008.06.200>.
- Gudmundsson, M.T., Hognadóttir, T., 2007. Volcanic systems and calderas in the Vatnajökull region, central Iceland: constraints on crustal structure from gravity data. *J. Geodyn.* 43, 153–169.
- Guillen, A., Menichetti, V., 1984. Gravity and magnetic inversion with minimization of a specific functional. *Geophysics* 49, 1354–1360.
- Guillou, H., Carracedo, J.C., Pérez Torrado, F., Rodríguez Badiola, E., 1996. K-Ar ages and magnetic stratigraphy of a hotspot-induced, fast grown oceanic island: El Hierro, Canary Islands. *J. Volcanol. Geoth. Res.* 73 (1–2), 141–155. [https://doi.org/10.1016/0377-0273\(96\)00021-2](https://doi.org/10.1016/0377-0273(96)00021-2).
- Hansteen, T.H., Kluegel, A., Schmincke, H.-U., 1998. Multi-stage magma ascent beneath the Canary Islands: Evidence from fluid inclusions. *Contrib. Mineral. Petrol.* 132 (1), 48–64. <https://doi.org/10.1007/s004100050404>.
- Hofmann-Wellenhoff, B., Lichtenegger, H., Wasle, E., 2008. GNSS-global Navigation Satellite Systems: GPS, GLONASS, Galileo, and More. Springer-Verlag Wien, p. 516. <https://doi.org/10.1007/978-3-211-73017-1>.
- Holcomb, R.T., Searle, R.C., 1991. Large landslides from oceanic volcanoes. *Mar. Geotechnol.* 10 (1–2), 19–32. <https://doi.org/10.1080/10641199109379880>.
- IGN, 2010. *El Nuevo modelo de geoide para España EGM08-REDNAP*. Centro de Observaciones Geodésicas, Instituto Geográfico Nacional, Madrid, p. 21 [in Spanish].
- Jiang, S., Wang, G., Li, S., Wang, G., Li, X., Zhang, H., Zhang, W., Cao, W., Dai, L., Suo, Y., Somerville, I., 2020. Potential deep-buried petroleum systems in Meso-Neoproterozoic rifts of the southwestern North China Craton revealed by gravity anomalies. *Precambrian Res.* 346, 105764.
- Krahenbuhl, R.A., Li, Y., 2006. Inversion of gravity data using a binary formulation. *Geophys. J. Int.* 167, 543–556.
- Kauahikaua, J., Hildenbrand, T., Webring, M., 2000. Deep magmatic structures of Hawaiian volcanoes, imaged by three-dimensional gravity models. *Geology* 28 (10), 883–886.
- Last, B.J., Kubik, K., 1983. Compact gravity inversion. *Geophysics* 48, 713–721.
- Lelièvre, P.G., Oldenburg, D.W., 2009. A comprehensive study of including structural information in geophysical inversions. *Geophys. J. Int.* 178, 623–637.
- Lelièvre, P.G., Farquharson, C.G., Hurich, C.A., 2012. Joint inversion of seismic traveltimes and gravity data on unstructured grids with application to mineral exploration. *Geophysics* 77, K1–K15.
- Li, Y., Oldenburg, D.W., 1998. 3-D inversion of gravity data. *Geophysics* 63 (1), 109–119.
- Linde, N., Ricci, T., Baron, L., Shakas, A., Berrino, G., 2017. The 3-D structure of the Somma-Vesuvius volcanic complex (Italy) inferred from new and historic gravimetric data. *Sci. Rep.* 7, 8434. <https://doi.org/10.1038/s41598-017-07496-y>.
- Linford, N., 2006. The application of geophysical methods to archaeological prospection. *Rep. Prog. Phys.* 69, 2205–2257.
- Liu, S., Jin, S., 2020. 3-D gravity anomaly inversion based on improved guided fuzzy C-means clustering algorithm. *Pure Appl. Geophys.* 177, 1005–1027.
- MacFarlane, D.J., Ridley, W.I., 1968. An interpretation of gravity data for Tenerife, Canary Islands. *Earth Planet Sci. Lett.* 4 (6), 481–486. [https://doi.org/10.1016/0012-821X\(68\)90029-0](https://doi.org/10.1016/0012-821X(68)90029-0).
- Mader, G.L., Bilich, A.L., 2012. Absolute Antenna Calibration at the US National Geodetic Survey. *AGU Fall Meeting Abstracts*, San Francisco, California, USA. G11B-0924.
- Magee, C., Stevenson, C.T.E., Ebmeier, S.K., Keir, D., Hammond, J.O.S., Gottsmann, J.H., Whaler, K.A., Schofield, N., Jackson, C.A.-L., Petronios, H.S., O'Driscoll, B., Morgan, J., Cruden, A., Vollgger, S.A., Dering, G., Micklithwaite, S., Jackson, M.D., 2018. Magma plumbing systems: a geophysical perspective. *J. Petrol.* 59 (6), 1217–1251. <https://doi.org/10.1093/petrology/egy064>.
- Martí, J., Castro, A., Rodríguez, C., Costa, F., Carrasquilla, S., Pedreira, R., Bolos, X., 2013. Correlation of magma evolution and geophysical Monitoring during the 2011–2012 El Hierro (Canary Islands) submarine eruption. *J. Petrol.* 54 (7), 1349–1373. <https://doi.org/10.1093/petrology/egt014>.
- Martins, C.M., Lima, W.A., Barbosa, V.C.F., Silva, J.B.C., 2011. Total variation regularization for depth-to-basement estimate: Part 1 -Mathematical details and applications. *Geophysics* 76 (1), I1–I12.

- Masson, D.G., 1996. Catastrophic collapse of the volcanic island of Hierro 15 ka ago and the history of landslides in the Canary Islands. *Geology* 24 (3), 231–234. <https://doi.org/10.1130/0091-7613>.
- Masson, D.G., Watts, A.B., Gee, M.J.R., Urgeles, R., Mitchell, N.C., Le Bas, T.P., Canals, M., 2002. Slope failures on the flanks of the western Canary Islands. *Earth Sci. Rev.* 57 (1–2), 1–35. [https://doi.org/10.1016/S0012-8252\(01\)00069-1](https://doi.org/10.1016/S0012-8252(01)00069-1).
- Mojica, O.F., Bassrei, A., 2015. Regularization parameter selection in the 3D gravity inversion of the basement relief using GCV: a parallel approach. *Comput. Geosci.* 82, 205–213.
- Molina-Garza, R., Urrutia-Fucugauchi, J., 1993. Deep crustal structure of central Mexico derived from interpretation of Bouguer gravity anomaly data. *Journal of Godynamics* 17 (4), 181–201.
- Montesinos, F.G., Armoso, J., Benavent, M., Vieira, R., 2006. The crustal structure of El Hierro (Canary Islands) from 3-D gravity inversion. *J. Volcanol. Geoth. Res.* 150 (1–3), 283–299. <https://doi.org/10.1016/j.jvolgeores.2005.07.018>.
- Oliveira, V.C., Barbosa, V.C.F., 2013. 3-D radial gravity gradient inversion. *Geophys. J. Int.* 195 (2), 883–902.
- Pallero, J.L.G., Fernández-Martínez, J.L., Fernández-Muñiz, Z., Bonvalot, S., Gabaldá, G., Nalpas, T., 2021. GRAVPSO2D: a Matlab package for 2D gravity inversion in sedimentary basins using the Particle Swarm Optimization algorithm. *Comput. Geosci.* 146, 104653. <https://doi.org/10.1016/j.cageo.2020.104653>.
- Pellicer, M.J., 1977. Estudio volcanológico de la Isla de El Hierro (islas canarias). *Estud. Geol.* 33 (2), 181–197 (In Spanish).
- Peltier, A., Bacheler, P., Staudacher, T., 2009. Magma transport and storage at Piton de La Fournaise (La Réunion) between 1972 and 2007: A review of geophysical and geochemical data. *J. Volcanol. Geotherm. Res.* 184, 93–108. <https://doi.org/10.1016/j.jvolgeores.2008.12.008>.
- Pick, M., Picha, J., Vyskocil, V., 1973. *Theory of the Earth's Gravity Field*. Elsevier, Amsterdam, p. 538pp.
- Rymer, H., Brown, G.C., 1986. Gravity fields and the interpretation of volcanic structures: geological discrimination and temporal evolution. *J. Volcanol. Geoth. Res.* 27 (3), 229–254. [https://doi.org/10.1016/0377-0273\(86\)90015-6](https://doi.org/10.1016/0377-0273(86)90015-6).
- Ryan, M.P., 1987. Elasticity and contractancy of Hawaiian olivine tholeiite and its role in the stability and structural evolution of subcaldera magma reservoirs and rift systems. In: Decker, R.W., Wright, T.L., Stauffer, P.H. (Eds.), *Volcanism in Hawaii: U.S. Geological Survey Professional Paper 1350*, Washington, USA, pp. 1395–1447.
- Prieto, J.F., González, P.J., Seco, A., Rodríguez-Velasco, G., Tunini, L., Perlock, P.A., Arjona, A., Aparicio, A., Camacho, A.G., Rundle, J.B., Tiampo, K.F., Pallero, J.L.G., Pospiech, S., Fernández, J., 2009. Geodetic and structural research in La Palma, Canary Islands, Spain: 1992–2007 results. *Pure Appl. Geophys.* 166, 1461–1484. <https://doi.org/10.1007/s00024-009-0505-2>.
- Sainz-Maza, S., Montesinos, F.G., Martí, J., Armoso, J., Calvo, M., Borreguero, A., 2017. Structural interpretation of El Hierro (Canary Islands) rifts system from gravity inversion modelling. *Tectonophysics* 712–713, 72–81. <https://doi.org/10.1016/j.tecto.2017.05.010>.
- Santos, D.F., Silva, J.B.C., Martins, C.M., Santos, R.C.S., Ramos, L.C., Araújo, A.C.M., 2015. Efficient gravity inversion of discontinuous basement relief. *Geophysics* 80 (4), G95–G106.
- Schmincke, H.D., 1976. The geology of the canary islands. In: Kunkel, G. (Ed.), *Biogeography and Ecology of the Canary Islands*. Springer Lunk, Dordrecht, pp. 67–184.
- Shamsipour, P., Marcotte, D., Chouteau, M., 2012. 3D stochastic joint inversion of gravity and magnetic data. *J. Appl. Geophys.* 79, 27–37.
- Silva Dias, F.J.S., Barbosa, V.C.F., Silva, J.B.C., 2011. Adaptive learning 3D gravity inversion for salt-body imaging. *Geophysics* 76 (3), 149–157.
- Tarantola, A., 1988. *The Inverse Problem Theory: Methods for Data Fitting and Model Parameter Estimation*. Elsevier, Amsterdam, p. 613pp.
- Tibaldi, A., 2015. Structure of volcano plumbing systems: a review of multi-parametric effects. *J. Volcanol. Geoth. Res.* 298, 85–135. <https://doi.org/10.1016/j.jvolgeores.2015.03.023>.
- Urgeles, R., Canals, M., Baraza, J., Alonso, B., Masson, D.G., 1997. The most recent megaland slides of the Canary Islands: El Golfo debris avalanche and Canary debris flow, west El Hierro Island. *Journal of Geophysical Research, Solid Earth* 102 (B9), 20305–20323. <https://doi.org/10.1029/97JB00649>.
- Vatankhah, S., Ardestani, V.E., Niri, S.S., Renaut, R.S., Kabirzadeh, H., 2019. IGUG: a MATLAB package for 3D inversion of gravity data using graph theory. *Comput. Geosci.* 128, 19–29. <https://doi.org/10.1016/j.cageo.2019.03.008>.
- Walker, G.P.L., 1999. Volcanic rift zones and their intrusion swarms. *J. Volcanol. Geoth. Res.* 94 (1–4), 21–34. [https://doi.org/10.1016/S0377-0273\(99\)00096-7](https://doi.org/10.1016/S0377-0273(99)00096-7).
- Wildman, R.A., Gazonas, G.A., 2009. Gravitational and magnetic anomaly inversion using a tree-based geometry representation. *Geophysics* 74, I23–I35.
- Zadro, M., Braatenberg, C., 1997. Spectral methods in gravity inversion: the geopotential field and its derivatives. *Ann. Geofisc.* XL (5), 1433–1443.